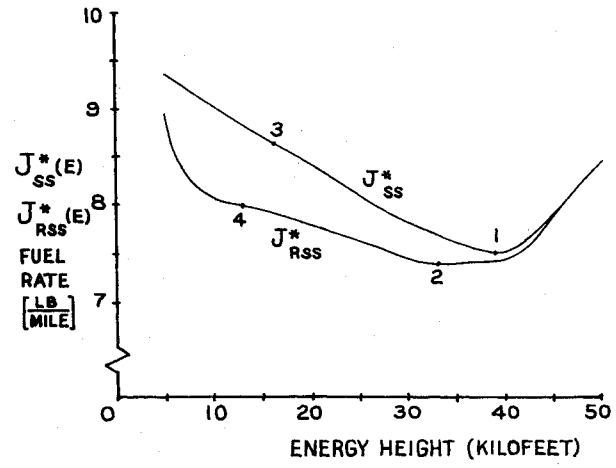

Fig. 1 Fuel consumption for F-4 in steady-state and relaxed steady-state cruise.

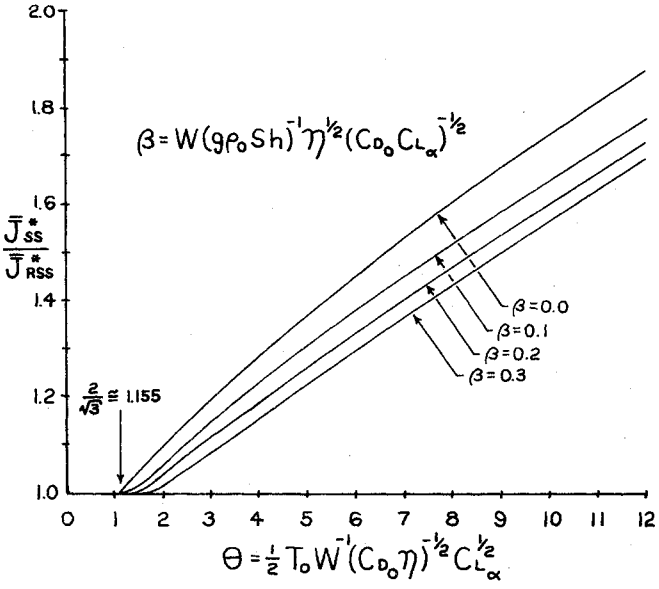

Fig. 2 Ratio of steady-state and relaxed steady-state cruise fuel rates.

thrust powered climb at $\bar{h}=\bar{h}_p$. For fixed $\bar{E}$ and $\bar{h}_p$ this leads to

$$\bar{J}_{RSS}=\bar{J}^*_{SS}(\tfrac{1}{2})(3)^{\frac{1}{4}}\theta\{\psi(\bar{E})\,[2\theta-(\bar{E}-\bar{h}_p) - (\bar{E}-\bar{h}_p)^{-1}e^{2\beta\bar{h}_p}]+e^{\beta\bar{h}_p}\}^{-1}(\bar{E}-\bar{h}_p)^{1/2} \quad (16)$$

where

$$\psi(\bar{E})=(\bar{E}+\bar{E}^{-1})^{-1} \text{ for } \bar{E}\geq 1,$$

$$\psi(\bar{E})=\tfrac{1}{2} \text{ for } \bar{E}<1, \text{ and } \theta=\bar{T}_0(2\delta)^{-1}$$

Minimizing J_{RSS} with respect to $\bar{E}$ and $\bar{h}_p$ determines $\bar{J}^*_{RSS}$. This has been carried out numerically for different values of the nondimensional parameters θ and β and the results are shown in Fig. 2.

For all $\theta>2(3)^{-1/2}\cong 1.155$ the RSS produces an improvement. For $\theta=2(3)^{-1/2}$ there is only enough thrust to produce the classical cruise, Eq. (14), at $\bar{h}=0$, and $\bar{J}^*_{SS}=\bar{J}^*_{RSS}$. For $\beta=0$, the optimum $\bar{E}=1$ for all θ and approximate formulas can be derived to give $\bar{h}_p\cong-(2\theta-1)/3$ and,

$$(\bar{J}^*_{RSS})^{-1}\bar{J}^*_{SS}\cong(2)^{5/2}(3)^{-9/4}\theta^{-1} \times(1+\theta)^{3/2}[1-9(1+\theta)^{-2}/8] \quad (17)$$

The errors in this $\bar{h}_p$ and Eq. (17) are very small for $\theta\geq 5$; the worst errors are for $\theta<2$ and are about 0.2 for $\bar{h}_p$ and 0.001 for Eq. (17). For $\beta>0$, $\bar{h}_p$ decreases slightly and $\bar{E}$ depends on $\theta(\bar{E}<1.2$ for $\theta\geq 2$ and $0\leq\beta\leq 0.3)$.

Figure 2 indicates the range of parameters where oscillatory aircraft motion is most likely to reduce fuel consumption. The most critical parameter is θ, which can be interpreted as the ratio of maximum engine thrust to minimum drag, both evaluated at the constraint altitude. Thus low-drag, high-thrust aircraft are favored. The parameter β is affected most strongly by wing loading, and aircraft with low wing loading are favored.

Conclusions

It has been shown that the methodology of optimal periodic control is useful in analyzing the dynamics of aircraft cruise. Relaxed steady-state analysis suggests that oscillatory aircraft motion may reduce fuel consumption, particularly when altitude constraints are imposed. Aircraft with high thrust to drag ratios and low wing loading are favored.

Proving conclusively that substantial improvements can be attained requires additional analysis and computations with more elaborate aircraft models. This work is under way and will be reported in the future.

References

[1]Bryson, A.E., Jr., Desai, M.N., and Hoffman, W.C., "Energy-State Approximation in Performance Optimization of Supersonic Aircraft," *Journal of Aircraft*, Vol. 6, Nov.-Dec. 1969, pp. 481-488.

[2]Zagalsky, N.R., Irons, R.P., Jr., and Schultz, R.L., "Energy State Approximation and Minimum-Fuel Fixed-Range Trajectories," *Journal of Aircraft*, Vol. 8, June 1971, pp. 488-490.

[3]Schultz, R.L. and Zagalsky, N.R., " Aircraft Performance Optimization," *Journal of Aircraft*, Vol. 9, Feb. 1972, pp. 108-114.

[4]Speyer, J.L., "On the Fuel Optimality of Cruise," *Journal of Aircraft*, Vol. 10, Dec. 1973, pp. 763-765.

[5]Schultz, R.L., "Fuel Optimality of Cruise," *Journal of Aircraft*, Vol. 11, Sept. 1974, pp. 586-587.

[6]Speyer, J.L., "A Test for Fuel Optimality of the Steady-State Cruise," to appear in the *AIAA Journal*.

[7]Bailey, J.E., "Periodic Operation of Chemical Reactors: A Review," *Chemical Engineering Communications*, Vol. 1, 1973, pp. 111-124.

[8]Guardabassi, G., Locatelli, A., and Rinaldi, S., "Status and Periodic Optimization of Dynamical Systems," *Journal of Optimization Theory and Applications*, Vol. 14, July 1974, pp. 1-20.

[9]Gilbert, E.G., "Vehicle Cruise: Improved Fuel Economy by Periodic Control," to appear in *Automatica*, 1976.

[10]Bittani, S., Fronza,G., and Guardabassi, G., "Periodic Control: A Frequency Domain Approach," *IEEE Transactions on Automatic Control*, Vol. AC-18, Feb. 1973, pp. 33-38.

[11]Bailey, J.E. and Horn, F.J.M.," Comparison Between Two Sufficient Conditions for Improvement of an Optimal Steady-State Process by Periodic Operation," *Journal of Optimzation Theory and Applications*, Vol. 7, May 1971, pp. 378-389.

[12]Stephen, P.W. and Chandler, W.J., "Simultation Evaluation of Flight Command Functions," Hughes Aircraft Co., Los Angeles, Calif., Report AFFDL-TR-70-4, March 1970.

Monitoring Wake Vortex Strength Decay Near the Ground

James N. Hallock*
DOT/Transportation Systems Center, Cambridge, Mass.

As part of an extensive program[1,2] to monitor the behavior of wake vortices in the terminal environment, the strength or circulation of vortices is being determined for aircraft landing on runway 31R at the John F. Kennedy International Airport in New York. An array of monostatic

Presented as Paper 75-882 at the AIAA 8th Fluid and Plasma Dynamics Conference, Hartford, Conn., June 16-18, 1975; submitted June 30, 1975; revision received March 31, 1976.

Index category: Jets, Wakes, and Viscid-Inviscid Flow Interactions.

*Engineer, Wake Vortex Program. Member AIAA.

acoustic sensors[3] is being used to measure vortex velocity fields; successive measurements of the velocity field of the same vortex are obtained as the vortex passes over each sensor. The sensor array is 2400 ft (731.5 m) from the displaced threshold of runway 31R and is aligned perpendicularly to the flight path of an aircraft landing on the runway. The sensors are located 200, 400, 600, and 800 ft (61, 122, 183, and 243 m) from the extended runway centerline.

Vortices generate substantial vertical winds but the ambient wind has little vertical component. The monostatic acoustic sensors transmit pulses of energy into a narrow vertical beam and the energy backscattered (incoherent scattering from temperature fluctuations) is detected and analyzed for Doppler shifts. Vortex height is indicated by the range gate with the largest Doppler shifts before and after the vortex passes over the sensor. Normally the transmitted pulse is 20 msec long and the pulse repetition period is 400 msec; these values give a range resolution of about 11 ft (3.3 m) and a maximum range of about 220 ft (67 m).

The vertical velocity distributions are used to calculate an "effective" strength. The "effective" strength is the circulation of an equivalent line vortex producing the same torque on a wing as would be produced by the measured vortex velocities. In other words, the first moment of the measured vertical velocity distribution is equated to the first moment of a potential or line vortex

$$\int_{-b/2}^{b/2} V_{\text{potential}} r \, dr = \int_{-b/2}^{b/2} V_{\text{measured}} r \, dr$$

Since

$$V_{potential} = \Gamma/(2\pi r), \qquad \Gamma = \frac{2\pi}{b} \int_{-b/2}^{b/2} V_{\text{measured}} r \, dr$$

where Γ is the "effective" strength, b is the wingspan of the hypothetical vortex-encountering aircraft, and V_{measured} are the vertical velocities.

To perform the integration, the radial parameter is transformed to time as the measured velocities are recorded as time histories. Thus, $r = V_T t$ where V_T is the horizontal transport velocity of a vortex over each sensor (obtained by noting the times at which the vortex is directly over each sensor and assuming a constant transport velocity between sensors). The wingspan b is an insensitive parameter; the value of the effective strength stabilizes as all the vorticity appears to be confined within 100 ft (30 m) of the vortex center.

Figures 1-3 show examples of the data, each figure exhibiting an apparently different but equally probable mode of decay. Up to four independent measurements of effective vortex strength can be made for each vortex (noisy channels often precluded obtaining all four measurements). Solid lines in Figs. 1-3 connect the data points for the same vortex. In Fig 1, four of the cases have been extended with broken lines; here the vortex was not seen in the following sensor because the strength decayed below the instrumental threshold.

Figure 1 displays cases where the strength very rapidly decays. Once the rapid decay commences, the strength is seen to decrease by a factor of two in approximately 15 sec. Two trends have been observed: 1) the rapid decay begins sooner and it occurs more often when the ambient turbulence is high, and 2) for a given turbulence level, the larger aircraft begin the rapid decay later than the smaller aircraft. It is suggested that the rapid decay is caused by a sinusoidal instability in which the vortex has linked with its image vortex.

Gradual decay is depicted in Fig. 2. The strength appears to slowly erode to a negligible value (at least, below the instrumental threshold) with a halving of strength every 30-60 sec. The dissipation of the vortex varies as t^{-1} and is probably a turbulent diffusion process.

Figure 3 exhibits a third mechanism: the vortex experiences a rapid decay which ultimately is curtailed leaving a relatively constant, but weaker, vortex in its stead. It is suggested that vortex breakdown, or core bursting, has occurred, leaving

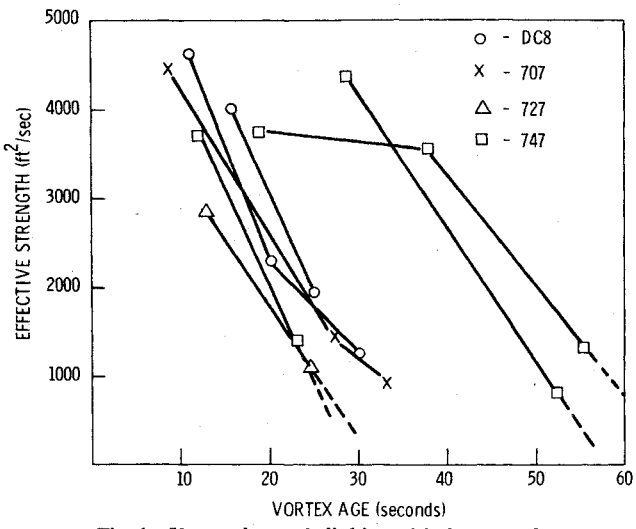

Fig. 1 Vortex decay via linking with the ground.

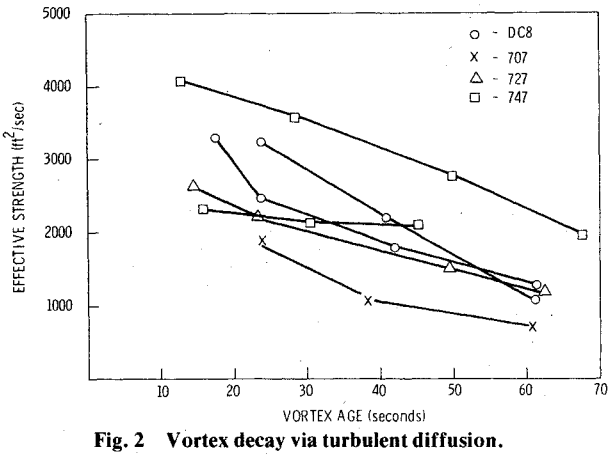

Fig. 2 Vortex decay via turbulent diffusion.

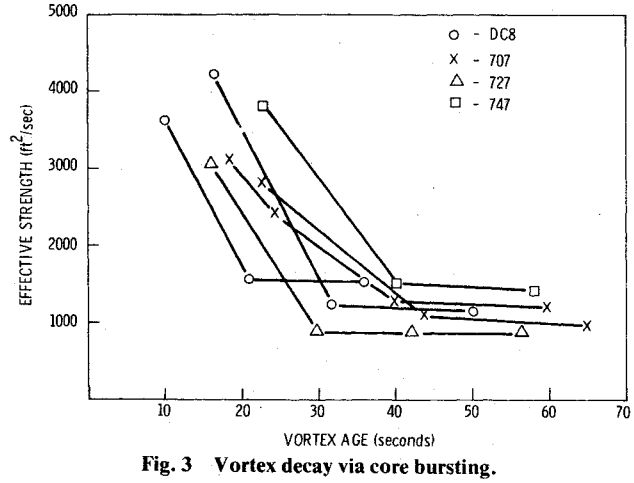

Fig. 3 Vortex decay via core bursting.

behind a remnant which mixes very little with the atmosphere. The strength of the remnant correlates with the size of the vortex generating aircraft: B-727 remnants are weaker than B-747 remnants. (In flight tests where smoke has been injected into the cores of the vortices, often after a vortex has "burst" a smaller core becomes discernable as smoke is transported by the axial flow in the vortex from an unburst portion to the remnant.)

Atmospheric winds appear to play an important part in the decay of a vortex. The strengths of vortices measured in winds above 10 knots tend to be less than strengths in light winds. It is suspected that the turbulence associated with the higher winds acts to dissipate the vortices. However, for winds in the

5-10 knot range very little trend is seen; both the port and starboard vortices appear to be dissipating at the same rate, even though one vortex is translating faster than wind and the other is translating slower than wind. In winds above 10 knots B-737 and DC-9 vortices were observed to decay quickly (in about 10 sec.).

References

[1]Hallock, J. N., Wood, W. D., and Spitzer, E. A., "The Motion of Wake Vortices in the Terminal Environment," *Proceedings of the AIAA/AMS Sixth Conference on Aerospace and Aeronautical Meteorology*, 1974, pp. 393-398.

[2]Hallock, J. N. and Wood, W. D., "Status of the Wake Vortex Avoidance System," *Proceedings of the IEE Electronics and Aerospace Systems Conference*, 1974, pp. 250-256.

[3]Burnham, D.C., Sullivan, T. E., and Wilk, L. S., "Measurement of Wake Vortex Strength by Means of Acoustic Back Scattering," *Journal of Aircraft*, to be published.

Aeroelastic Stability and Control of an Oblique Wing: Wind Tunnel Experiments

R. T. Jones*
NASA Ames Research Center, Moffett Field, Calif.

AEROELASTIC stability and control of an oblique wing has proved to be a conceptually difficult problem. Intuitively, one expects the forward panel of the oblique wing to behave as a conventional swept forward wing panel. If this were the case, then the oblique-winged airplane would suffer a loss of aileron control and aeroelastic divergence at a relatively low value of the dymanic pressure.

A more careful theoretical analysis, by the author and J. W. Nisbet of the Boeing Company, which includes freedom of the aircraft fuselage in roll shows that the behavior of the oblique wing is different from that of swept forward wings. The analysis shows that the oblique wing does not have the divergent instability of the swept forward wing but can be operated safely at much higher dynamic pressures. Moreover the aileron control, which would show singular behavior on approaching the dynamic pressure for divergence of the swept forward wing, remains effective according to this theory up to considerably higher values of the dynamic pressure. If q^* is the dynamic pressure for divergence with the fuselage fixed in roll and q is the dynamic pressure for instability with the fuselage free then the ratio q/q^* may be shown to depend on the mass distribution and inertia of the wing in relation to the moment of inertia of the fuselage about its roll axis. The predicted form of instability is a bending oscillation of the wing coupled with oscillatory rolling motion of the fuselage.

These predictions of the theory have now been verified in wind tunnel tests of an elastic wing model made by Dennis W. Riddle and Peter Gaspers at NASA-Ames Research Center. Figures 1 and 2 show the model installed in the 7′ × 10′ wind tunnel of the U. S. Army Air Mobility Laboratory at Ames. These experiments will be covered more completely in a later report.

The model wing has an elliptic planform of 10 to 1 axis ratio and a symmetrical airfoil section of 7-1/2% thickness/chord ratio. The wing is of wood and as may be seen in the photographs, slack wires were used to limit the amplitude of unstable motions. The fuselage was mounted on bearings permitting freedom in roll, but provision was made

Received Sept., 26, 1974; revision received Jan., 12, 1976.

Index categories: Aircraft Configuration Design; Aircraft Handling, Stability and Control; Aircraft Structural Design (including Loads).

*Senior Staff Scientist. Fellow AIAA.

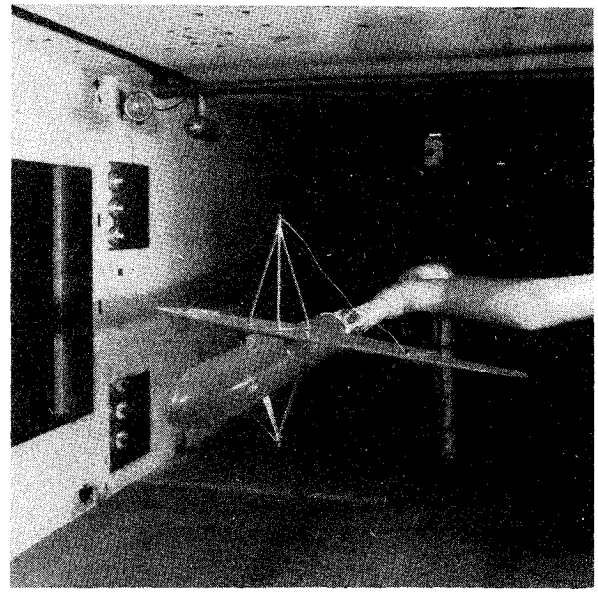

Fig. 1 Aeroelastic model in 7 ft × 10 ft wind tunnel.

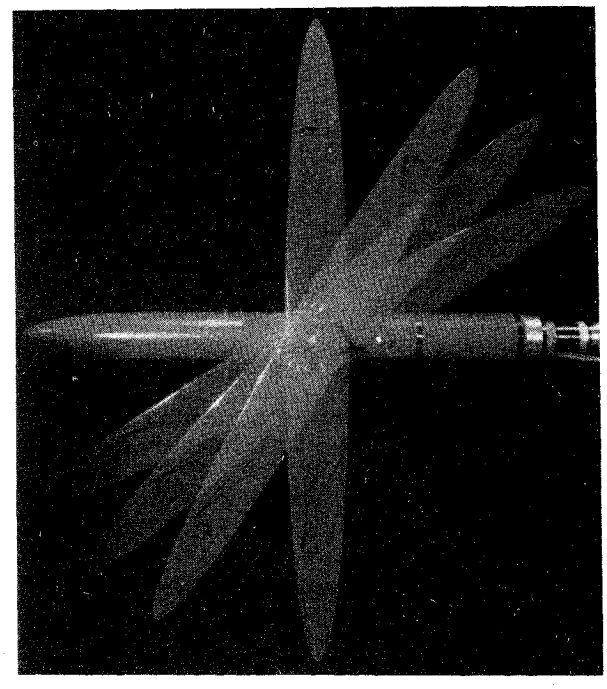

Fig. 2 Plan view of aeroelastic model.

to clamp the fuselage for some of the tests. The ailerons were actuated remotely by a Craft radio control unit of the type used by RC model flyers.

With the fuselage clamped and the model at a fixed positive angle of attack the upward deflection of the wing increased progressively with increasing airspeed. By extrapolating the deflection curve of the forward wing panel, it was determined that static divergence would occur at a speed of approximately 225 fps. The divergence speed was nearly the same at 45° and 60° yaw. With the model free in roll and with ailerons activated to maintain trim the model developed unstable bending-rolling oscillations at a speed of 275 fps again at either 45° or 60° yaw. Thus, freedom in roll increased the dynamic pressure at which aeroelastic instability first appeared by approximately 50%, in rough agreement with the behavior predicted by our analytical model. With the model free in roll, the effectiveness of the ailerons in maintaining trim was not noticeably affected by passage through the speed at which the wing would have become unstable if clamped.